Frequency-domain method for non-stationary stochastic vibrations of train-bridge coupled system with time-varying characteristics

Simian Lei[1], Yaojun Ge[1], Qi Li[1*], David J. Thompson[2]

[1] Department of Bridge Engineering, Tongji University

1239 Siping Road, Shanghai, China

[2] Institute of Sound and Vibration Research, University of Southampton,

Southampton SO17 1BJ, United Kingdom

Abstract

When a train passes over a bridge, the vibrations of the vehicles and the bridge are the result of non-stationary stochastic processes due to the time-dependent characteristics of the coupled vehicle-bridge system. The aim of this study is to generalize the frequency domain method to investigate the non-stationary random vibration of the coupled system subjected to the excitation of track irregularities with consideration of time-dependent characteristics. To illustrate the method, a three-span simply supported bridge traversed by a single railway vehicle is adopted as an example. The time-dependent frequency response function (FRF) of the coupled system is theoretically derived through solving ordinary differential equations with variable complex coefficients, and the perturbation method is adopted to improve the calculation efficiency. By combining this with Priestley's Evolutionary Spectra theory, the evolutionary power spectral density (PSD) of the non-stationary random response of the system is then derived. The transitions occurring when the wheels cross the joints between each bridge span and between the bridge and the adjacent roadway. By adopting mode shapes of the full structure, the change of states of the vehicle crossing multiple bridge spans and moving onto the roadway can be solved as a continuous process without separation. The proposed method is validated by comparisons with the Monte Carlo method, showing higher accuracy and efficiency when calculating the time-varying standard deviation of the response. It is found that the vibration of the vehicle is approximately stationary but with large variance due to the random track irregularities, while the bridge vibration follows a strongly non-stationary process with small randomness and is more related to the moving mass effect.

Keywords: vehicle-bridge system; track irregularity; frequency domain method; non-stationary stochastic vibrations; perturbation method; evolutionary power spectral density.

---

* Corresponding author, E-mail address: liqi_bridge@tongji.edu.cn (Q. Li).

This is the accepted manuscript version of the article.

The final published version of this article is available at https://doi.org/10.1016/j.ymssp.2022.109637

1 Introduction

When a train crosses a bridge, both the train and the bridge vibrate due to wheel and track irregularities, as well as due to the passage of the loads over the bridge. The vibration of such train-bridge coupled systems has been studied for many years with both deterministic and stochastic methods, by treating the coupled system as time dependent due to the motion of the vehicles across the bridge [1-3]. According to the theory of linear time-varying systems [4, 5], even if the track irregularity excitation of the coupled system is assumed as a stationary random process, the vibration of the system will be non-stationary [1]. This is especially true when other non-stationary excitations are considered in the system, e.g., earthquakes or extreme wind loads [2]. In view of the non-stationary characteristics, many attempts have been made to develop random vibration theory for the train-bridge coupled system. The studies of non-stationary random vibration of the train-bridge coupled system can be broadly classified into four categories.

The first category of methods is the one used by Fryba [6] considering a beam traversed by a random force with constant mean value at a constant speed. He concluded that the response of the beam results from a non-stationary process even if the force is a stationary signal. A subsequent study was carried out by Iwankiewicz and Śniady [7] considering random streams of traffic loads, of which the arrival times were assumed to be a Poisson process. In these studies, the vehicles were simplified as moving random forces caused by track or road irregularities.

The second class of methods is the Monte Carlo method (MCM) adopted to solve the train-bridge coupled system excited by random track irregularities. It uses time-history samples generated from the track irregularity power spectral density (PSD) and then computes the deterministic responses of the system in the time domain. Xia et al. [8] used this method to evaluate the dynamic performance of the train-bridge system under random irregularity samples and proposed reinforcement schemes for steel girders. Zhai et al. [9] has made significant contributions in the dynamic interactions of high-speed trains, and the track-bridge coupled system, mainly with the time-domain integration method based on Monte Carlo simulations [10-12]. To obtain reliable statistical characteristics of the system responses, sufficient samples and complex time-frequency analysis techniques should be employed, which are undoubtedly computationally intensive.

The third category of methods for investigating the non-stationary vibration in train-bridge coupled systems is the pseudo excitation method (PEM) developed by Lin et al. [13, 14], which can deal with the random vibration problem with either stationary or non-stationary excitations. It was originally developed for linear time-invariant

systems, e.g., the earthquake analysis of a bridge [14]. With this method, the non-stationary characteristics of the response can be conveniently obtained, including the time-dependent PSD and standard deviation (SD) [15, 16]. Recent studies have shown that it can be extended to linear time-dependent systems [1], e.g., the train-bridge coupled systems. Zhang et al. [2] considered the excitation due to stationary track irregularities and non-stationary horizontal earthquakes simultaneously and calculated the non-stationary random vibration of the train-bridge coupled system by means of the PEM. The Precise Integration Method can be combined with this process to improve the efficiency [2, 15, 16] when computing the corresponding time-history responses to the pseudo excitations.

The fourth category of methods is the probability density evolution method (PDEM) proposed by Li and Chen [17, 18], based on the principle of probability preservation. It can deal with the problems of linear and nonlinear stochastic vibration. Using the PDEM, Yu et al. [19] obtained the random vibration of a three-dimensional train–bridge coupled system considering random train parameters and rail irregularities, and discussed the effects of their randomness on the system responses. Compared with the MCM and PEM, the PDEM aims at obtaining the evolution of the probability density function (PDF) of the stochastic response. However, the second-order statistical quantities, especially the energy distribution of the response, cannot easily be obtained from this approach [20].

Frequency-domain methods can also be adopted but have not been reported for the random vibration analysis of the train-bridge coupled system. They are excluded from the aforementioned four methods because they were often believed only to be applicable to linear time-invariant systems. With frequency-domain methods the expected response spectra can be obtained directly by using algebraic methods without integration [21]. In contrast, the response of linear time-varying systems is usually solved through time-domain approaches, and even the PEM and PDEM could not avoid the integration process. It was Zadeh [4, 5] who first presented the time-variant frequency response function (FRF) to characterize the dynamic behaviour of linear time-varying systems, and showed that these preserved the significant properties of the FRF for linear time-invariant systems. With the help of the time-variant FRF, the response to any prescribed excitations could be obtained in a similar manner, and thus the frequency analysis of linear time-varying systems became possible. Inspired by this work, Pintelon et al. [22] investigated the dynamics of a linear system with smooth time-varying parameters and evaluated the non-stationary response to stochastic excitations. It should be noted that the energy distribution over frequency of the non-stationary response also retains time-dependent characteristics, and many attempts have

been made to apply power spectral analysis to non-stationary processes, including the instantaneous PSD [23], the wavelet spectrum [24], and the Hilbert spectrum [25]. These treatments however lack physical interpretation, i.e., local energy distributions over frequency as the usual definition for stationary processes, so that it is difficult to reverse the process and generate a copy of the original signal from these spectra. The conventional spectrogram assumes the signal to be stationary within a moving short window, so that the PSD can be evaluated within each window. This requires that the non-stationarity of the signal should not be too strong, and the window should not be too short (inadequate frequency resolution) or too long (inadequate time resolution), due to the Heisenberg uncertainty principle. Based on the spectral representation, Priestley [26, 27] established a theoretical definition of evolutionary spectra to describe the energy distribution of the non-stationary process over frequency at each instant of time. It was shown that the evolutionary spectra possess the same characteristics as the PSD of a stationary process, and can produce high time and frequency resolutions simultaneously. Therefore, by combining the theory of time-varying FRFs and the evolutionary spectra, it is possible to extend the frequency-domain method to deal with the non-stationary vibration of a linear time-varying system subjected to stochastic excitation.

The aim of this study is to use this frequency domain method to investigate the non-stationary random vibration of train-bridge coupled systems subjected to excitation by track irregularities. By way of illustration, a typical model of a multi-span railway bridge traversed by a high-speed railway vehicle is adopted as an example for modelling the train-bridge coupled system. To apply the frequency-domain method to this system, the linear time-varying system with multiple inputs and multiple outputs is first investigated, and the governing equations of the time-dependent FRFs are derived. As an improvement for computation efficiency, the perturbation method is adopted to obtain the time-dependent FRFs by keeping only the first three terms of the perturbation. The evolutionary PSD of the non-stationary random response is then derived by combining the time-dependent FRFs with Priestley's Evolutionary Spectra theory [26, 27]. Additionally, to consider the transitions occurring when the wheels of the vehicle cross the joints between each bridge span and between the bridge and the roadway, mode shapes of each span are adopted that are extended by zeros to cover the full structure, so that the whole process can be directly solved without separating each state. The proposed frequency-domain method is first validated by comparing the time-varying standard deviation and mean of the responses with those obtained from the Monte Carlo simulations. The evolutionary PSD of the non-stationary response is also evaluated based on the proposed method and then discussed in detail. Moreover, the

3σ rule [1] is adopted to estimate the extreme values of the non-stationary responses, and the influence of the track irregularities on the non-stationary responses of the system is investigated.

2 Frequency analysis of linear time-varying system

2.1 Time-dependent FRFs of a multi-input multi-output linear time-varying system

A linear time-varying (LTV) system with multiple inputs and outputs can be described by a set of non-homogeneous linear ordinary differential equations with coefficients that vary with time [4, 5]

$$\mathbf{L}(p;t)\mathbf{y}(t) = \mathbf{K}(p;t)\mathbf{u}(t) \tag{1}$$

in which $\mathbf{u}(t)$ is the input vector with s components, and $\mathbf{y}(t)$ is the output vector with r components. $\mathbf{L}(p;t)$ and $\mathbf{K}(p;t)$ are power series for the coefficients

$$\mathbf{L}(p;t) = \sum_{i=0}^{n_1} \mathbf{A}_i(t)p^i \tag{2}$$

$$\mathbf{K}(p;t) = \sum_{j=0}^{n_2} \mathbf{B}_j(t)p^j \tag{3}$$

in which $\mathbf{A}_i(t)$ is the $r \times r$ matrix of known time-varying coefficients of the outputs; $\mathbf{B}_j(t)$ is the $r \times s$ matrix of known time-varying coefficients of the inputs; and p is the differential operator

$$p = \frac{\mathrm{d}}{\mathrm{d}t} \tag{4}$$

Based on the principle of superposition for a linear system, when the system is subjected to any arbitrary inputs, the output can be determined by

$$\mathbf{y}(t) = \int_{-\infty}^{\infty} \mathbf{W}(t,\xi)\mathbf{u}(\xi)\mathrm{d}\xi \tag{5}$$

in which $\mathbf{W}(t,\xi)$ is an $r \times s$ matrix of impulse response functions and can be obtained from Eq. (1) by

$$\mathbf{L}(p;t)\mathbf{W}(t,\xi) = \mathbf{K}(p;t)\delta(t-\xi)\mathbf{I} \tag{6}$$

Note that the upper limit of the integral in Eq. (5) has been extended from t to ∞ since the impulse response functions are zero for $\xi > t$. Taking Fourier transforms and writing the Fourier transform of $\mathbf{u}(\xi)$ as $\mathbf{U}(\mathrm{j}\omega)$, and then exchanging the order of integration, Eq. (5) can be written as

$$\mathbf{y}(t) = \frac{1}{2\pi}\int_{-\infty}^{\infty} \mathbf{H}(\mathrm{j}\omega,t)\mathbf{U}(\mathrm{j}\omega)\mathrm{e}^{\mathrm{j}\omega t}\mathrm{d}\omega \tag{7}$$

where $\mathbf{H}(\mathrm{j}\omega,t)$ is the $r \times s$ matrix of the Fourier transforms of the impulse response functions $\mathbf{W}(t,\xi)$ with respect to the time shift $t-\xi$

$$\mathbf{H}(\mathrm{j}\omega,t) = \int_{-\infty}^{\infty} \mathbf{W}(t,\xi)\mathrm{e}^{-\mathrm{j}\omega(t-\xi)}\mathrm{d}\xi \tag{8}$$

Compared with the FRF of a linear time-invariant (LTI) system, $\mathbf{H}(\mathrm{j}\omega, t)$ can be regarded as a generalized form of the FRF that depends on the observation time t, and is defined as the time-dependent FRF matrix. Eq. (8) gives a theoretical definition of the time-dependent FRF of a time-varying system, which takes account of all impulse responses prior to the observation time. In contrast, conventional time-frequency analysis techniques assume the system as invariant within a moving short window [28], so that the problem reduces to finding the FRF of an equivalent LTI system within each window, which applies only to systems with slowly time-varying characteristics. It will be demonstrated that the proposed method also allows the system to be fast time-varying and, more importantly, allows abrupt transitions of state to occur.

2.2 Governing equation of time-dependent FRFs

In practice, $\mathbf{H}(\mathrm{j}\omega, t)$ is not determined by using Eq. (8), due to the inconvenience of obtaining the impulse response functions $\mathbf{W}(t, \xi)$ and evaluating the integral. This section will show that $\mathbf{H}(\mathrm{j}\omega, t)$ can be directly obtained from a linear differential equation [4].

By taking a Fourier transform with respect to ξ, Eq. (6) can be transformed to the time-frequency domain

$$\mathbf{L}(p; t)\left[\mathbf{H}(\mathrm{j}\omega, t)\mathrm{e}^{\mathrm{j}\omega t}\right] = \mathbf{K}(p; t)\mathrm{e}^{\mathrm{j}\omega t} \tag{9}$$

The polynomial derivatives of $\mathbf{H}(\mathrm{j}\omega, t)\mathrm{e}^{\mathrm{j}\omega t}$ can be determined by applying the chain rule

$$\mathbf{L}(p; t)\left[\mathbf{H}\mathrm{e}^{\mathrm{j}\omega t}\right] = \left[\mathbf{L}(p; t)\mathrm{e}^{\mathrm{j}\omega t}\right]\mathbf{H} + \left[\frac{\partial \mathbf{L}(p; t)}{\partial p}\mathrm{e}^{\mathrm{j}\omega t}\right]\frac{\mathrm{d}\mathbf{H}}{\mathrm{d}t} + \cdots + \left[\frac{1}{n_1!}\frac{\partial^{n_1}\mathbf{L}(p; t)}{\partial p^{n_1}}\mathrm{e}^{\mathrm{j}\omega t}\right]\frac{\mathrm{d}^{n_1}\mathbf{H}}{\mathrm{d}t^{n_1}} \tag{10}$$

noting that

$$\frac{\partial^{\mu}\mathbf{L}(p; t)}{\partial p^{\mu}}\mathrm{e}^{\mathrm{j}\omega t} = \frac{\partial^{\mu}\mathbf{L}(\mathrm{j}\omega; t)}{\partial(\mathrm{j}\omega)^{\mu}}\mathrm{e}^{\mathrm{j}\omega t} \quad (\mu = 0, 1, \cdots, n_1) \tag{11}$$

and

$$\mathbf{K}(p; t)\mathrm{e}^{\mathrm{j}\omega t} = \mathbf{K}(\mathrm{j}\omega; t)\mathrm{e}^{\mathrm{j}\omega t} \tag{12}$$

Substituting Eq. (10), Eq. (11) and Eq. (12) into Eq. (9), the governing equations for $\mathbf{H}(\mathrm{j}\omega, t)$ can be obtained as

$$\boldsymbol{\alpha}_{n_1}(\mathrm{j}\omega; t)\frac{\mathrm{d}^{n_1}\mathbf{H}}{\mathrm{d}t^{n_1}} + \cdots + \boldsymbol{\alpha}_1(\mathrm{j}\omega; t)\frac{\mathrm{d}\mathbf{H}}{\mathrm{d}t} + \boldsymbol{\alpha}_0(\mathrm{j}\omega; t)\mathbf{H} = \mathbf{K}(\mathrm{j}\omega; t) \tag{13}$$

in which

$$\boldsymbol{\alpha}_{\mu}(\mathrm{j}\omega; t) = \frac{1}{\mu!}\frac{\partial^{\mu}\mathbf{L}(\mathrm{j}\omega; t)}{\partial(\mathrm{j}\omega)^{\mu}} \tag{14}$$

It can be seen that $\mathbf{H}(\mathrm{j}\omega, t)$ is governed by a set of non-homogeneous linear ordinary differential equations with variable complex coefficients, of which the order is the same as that of Eq. (1) for the original LTV system.

2.3 Approximate solution for time-dependent FRFs

Once the time-dependent FRFs has been determined, the non-stationary response of an LTV system to any arbitrary inputs can be simply evaluated, but this may still need intensive calculations due to the efforts in determining the time-dependent FRFs by Eq. (13). This is especially true for LTV systems with large numbers of DOFs. Therefore, it is necessary to develop an approximate method for solving Eq. (13).

The perturbation method [29, 30] is widely used for finding an approximate solution to an unsolvable differential equation, by breaking the problem into solvable and perturbative parts. The solution can be expressed as a power series

$$\mathbf{H}(\mathrm{j}\omega, t) = \mathbf{H}_0(\mathrm{j}\omega, t) + \mathbf{H}_1(\mathrm{j}\omega, t) + \mathbf{H}_2(\mathrm{j}\omega, t) + \cdots \tag{15}$$

in which the first term is the known solution to the solvable problem and the successive perturbative terms describe the deviation in the solution. This method is especially applicable for systems with periodically varying parameters, in which Eq. (15) will converge rapidly so the approximate solution can be obtained by keeping only the first two terms.

For determining time-dependent FRFs with the perturbation method, the first step is to obtain the exact solution of a simpler initial problem by converting Eq. (13) into a differential equation with constant coefficients

$$\overline{\boldsymbol{\alpha}}_{n_1} \frac{\mathrm{d}^{n_1}\mathbf{H}_0}{\mathrm{d}t^{n_1}} + \cdots + \overline{\boldsymbol{\alpha}}_1 \frac{\mathrm{d}\mathbf{H}_0}{\mathrm{d}t} + \overline{\boldsymbol{\alpha}}_0 \mathbf{H}_0 = \mathbf{K}(\mathrm{j}\omega; t) \tag{16}$$

in which $\overline{\boldsymbol{\alpha}}_\mu$ is the mean value over t of $\boldsymbol{\alpha}_\mu(\mathrm{j}\omega; t)$.

Successive corrections to $\mathbf{H}_0(\mathrm{j}\omega, t)$ can then be obtained with an iterative procedure, by solving the equation

$$\overline{\boldsymbol{\alpha}}_{n_1} \frac{\mathrm{d}^{n_1}\mathbf{H}_k}{\mathrm{d}t^{n_1}} + \cdots + \overline{\boldsymbol{\alpha}}_1 \frac{\mathrm{d}\mathbf{H}_k}{\mathrm{d}t} + \overline{\boldsymbol{\alpha}}_0 \mathbf{H}_k = \mathbf{P}\{\mathbf{H}_{k-1}\} \tag{17}$$

in which $k = 1, 2 \cdots$

$$\mathbf{P}\{\mathbf{H}_{k-1}\} = \left[\overline{\boldsymbol{\alpha}}_{n_1} - \boldsymbol{\alpha}_{n_1}(\mathrm{j}\omega; t)\right] \frac{\mathrm{d}^{n_1}\mathbf{H}_{k-1}}{\mathrm{d}t^{n_1}} + \cdots + \left[\overline{\boldsymbol{\alpha}}_1 - \boldsymbol{\alpha}_1(\mathrm{j}\omega; t)\right] \frac{\mathrm{d}\mathbf{H}_{k-1}}{\mathrm{d}t} + \left[\overline{\boldsymbol{\alpha}}_0 - \boldsymbol{\alpha}_0(\mathrm{j}\omega; t)\right]\mathbf{H}_{k-1} \tag{18}$$

The k-th order perturbation ($k = 0, 1, 2 \cdots$) is defined in terms of the order to which the perturbation is carried out.

2.4 Evolutionary PSDs

According to Priestley's Evolutionary Spectra theory [26, 27], a non-stationary process can be represented in a generalized spectral representation form

$$X(t) = \int_{-\infty}^{\infty} H(\omega, t) \mathrm{e}^{\mathrm{j}\omega t} \mathrm{d}Z(\omega) \tag{19}$$

in which $H(\omega, t)$ is a deterministic time-frequency modulation function with complex values, and $Z(\omega)$ is a process with orthogonal increments. When $H(\omega, t)$ is 1, $X(t)$ will degrade into the corresponding stationary process $X_s(t)$, for which the power

spectral density function can be defined as

$$S_{X_s}(\omega) = \frac{\mathrm{E}[|\mathrm{d}Z(\omega)||\mathrm{d}Z(\omega)|]}{\mathrm{d}\omega} \tag{20}$$

where $\mathrm{E}[\cdot]$ denotes the expectation operator, and the evolutionary power spectral density (EPSD) of $X(t)$ can be defined as

$$S_X(\omega,t) = \frac{|H(\omega,t)|^2\mathrm{E}[|\mathrm{d}Z(\omega)||\mathrm{d}Z(\omega)|]}{\mathrm{d}\omega} = |H(\omega,t)|^2 S_{X_s}(\omega) \tag{21}$$

Due to the orthogonality of $Z(\omega)$, the evolutionary spectrum maintains the same properties as the power spectrum of a stationary process, such as determination of the time-varying variance

$$\sigma_X^2(t) = \int_{-\infty}^{\infty} S_X(\omega,t)\mathrm{d}\omega \tag{22}$$

The non-stationary process $X(t)$ can be regarded as the output of an LTV system with the input $X_s(t)$, and $H(\omega,t)$ is exactly the corresponding time-dependent FRF of the system. For the linear time-varying system described by Eq. (1), provided that the input $\mathbf{u}(t)$ is a stationary stochastic process with constant mean $\boldsymbol{\mu}_\mathbf{u}$, the EPSD matrix for the output $\mathbf{y}(t)$ can be derived as

$$\mathbf{S}_\mathbf{y}(\omega,t) = \mathbf{H}^*(\mathrm{j}\omega,t)\mathbf{S}_\mathbf{u}(\omega)\mathbf{H}^\mathrm{T}(\mathrm{j}\omega,t) \tag{23}$$

in which $\mathbf{S}_\mathbf{u}(\omega)$ is the spectral density matrix for the input, the superscript * denotes the conjugate and superscript T denotes the transpose operation. The time-varying covariance matrix of $\mathbf{y}(t)$ is obtained as

$$\mathrm{cov}[\mathbf{y}(t)] = \int_{-\infty}^{\infty} \mathbf{H}^*(\mathrm{j}\omega,t)\mathbf{S}_\mathbf{u}(\omega)\mathbf{H}^\mathrm{T}(\mathrm{j}\omega,t)\mathrm{d}\omega \tag{24}$$

It is noted that the mean of $\mathbf{y}(t)$ at each instant of time will no longer be a constant value, unless $\boldsymbol{\mu}_\mathbf{u} = \mathbf{0}$. This can be proved based on Eq. (5)

$$\boldsymbol{\mu}_\mathbf{y}(t) = \int_{-\infty}^{\infty} \mathbf{W}(t,\xi)\mathrm{E}[\mathbf{u}(\xi)]\mathrm{d}\xi = \int_{-\infty}^{\infty} \mathbf{W}(t,\xi)\boldsymbol{\mu}_\mathbf{u}\mathrm{d}\xi \tag{25}$$

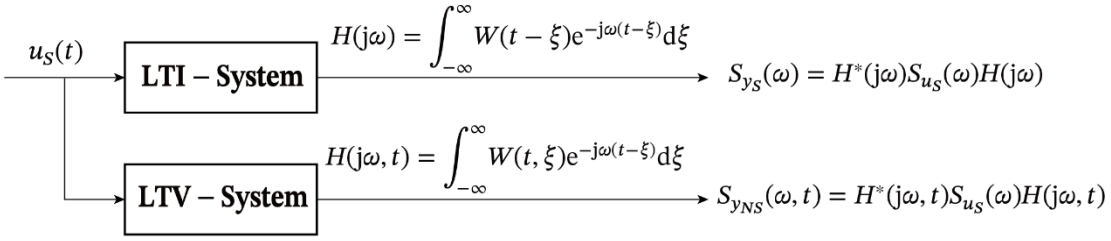

Fig. 1. Comparison between the frequency-domain methods for the linear time-invariant (LTI) system and the linear time-varying (LTV) system.

Fig. 1 gives a comparison between the frequency-domain methods for calculating stochastic vibrations of an LTI system and an LTV system subjected to stationary stochastic excitations. Recently, Xiao et al. [31, 32] developed a wavelet-expansion

based method which could efficiently evaluate the time-varying PSD of stochastic responses of a time-varying system. In essence, this is a numerical method: the non-stationary responses are approximated by a summation of harmonic functions [33] with different scales and time shifts in a prescribed finite time duration. Thus, periodic generalized harmonic wavelets, and the wavelet coefficients as well as the response spectra are calculated at discrete frequency points and time instants. In contrast, the proposed method is a theoretical method. It is seen from Fig. 1 that, based on the Priestley's Evolutionary PSD, the theoretically derived time-dependent FRF of the LTV system can be used to obtain the stochastic response in a similar manner as for an LTI system, so that the proposed method can be regarded as a natural extension of the conventional frequency-domain method.

3 Analysis of train-bridge coupled system

In this section, the frequency domain methods proposed in Section 2 are employed to derive the EPSDs for the responses of the railway vehicle-bridge coupled system (see Fig. 2) excited by random roughness or irregularities.

3.1 Train-bridge coupled model

In order to focus on the methodology and simplify the illustration, a single railway vehicle is considered in this study to cross a multi-span bridge with stationary track irregularities. The single vehicle model consists of a car body, two bogie frames, four wheelsets and several flexible spring-damper elements connecting them [21], as shown in Fig. 2, in which m_b and J_b are the mass and the moment of inertia for the car body; m_t and J_t are the mass and the moment of inertia for the bogie frame; m_w is the mass of the wheelset; k_2 and c_2 are the vertical stiffness and damping of the secondary suspension; k_1 and c_1 are the vertical stiffness and damping of the first suspension; a is the half distance between the secondary suspensions, and b is the half distance between the two wheelsets of each bogie. The car body, bogie frames, and wheelsets are regarded as rigid bodies [34], and only vibration in the vertical direction is considered.

It is noted that the magnitude of the track transfer receptance from one wheel position to another is far lower than that of the point receptance at frequencies below 200 Hz, due to the high track decay rates in this frequency region [35]. Therefore, the track is neglected in this model and its point receptance is considered by tuning the vertical stiffness k_c and damping c_c of the equivalent wheel-rail contact spring to include track flexibility. The bridge is represented by a multi-span simply supported Euler beam, with m representing the mass per unit length, EI the bending stiffness, and c_b the damping coefficient of the beam; l is the length of each span of the bridge, and S is the number of spans. Each span is considered uncoupled from the others. In

fact, this model can be extended to any bridge type by adopting the modal coordinates, as will be demonstrated in the following derivations.

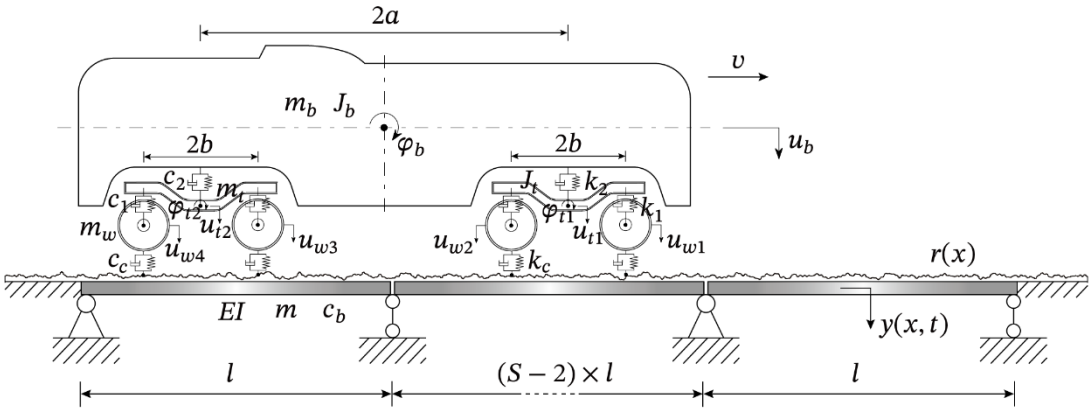

Fig. 2. Ten-DOF model of a railway vehicle running on a multi-span railway bridge with stationary track irregularities.

Based on the aforementioned assumptions, the vehicle model has a total of ten degrees of freedom (DOFs), including seven translational and three rotational DOFs, which are referenced from the static-equilibrium position. The equation of motion for the vehicle subsystem can be expressed as

$$\mathbf{m}_v\ddot{\mathbf{u}}_v + \mathbf{c}_v\dot{\mathbf{u}}_v + \mathbf{k}_v\mathbf{u}_v = -\mathbf{f} \tag{26}$$

in which $\mathbf{m}_v$, $\mathbf{c}_v$ and $\mathbf{k}_v$ are the mass, damping, and stiffness matrices for the vehicle, which are given in Appendix A; $\mathbf{u}_v$ is the displacement vector of the vehicle

$$\mathbf{u}_v = \{u_b \quad \varphi_b \quad u_{t1} \quad \varphi_{t1} \quad u_{t2} \quad \varphi_{t2} \quad u_{w1} \quad u_{w2} \quad u_{w3} \quad u_{w4}\}^{\mathrm{T}} \tag{27}$$

in which u_{b}, u_{ti} and u_{wj} are the vertical displacements of the car body, the i-th bogie, and j-th wheelset ($i = 1,2$ and $j = 1,2,3,4$); φ_b and φ_{ti} are the pitch displacements of the car body and i-th bogie; $\mathbf{f}$ is the vector of interaction forces between the wheelsets and the bridge

$$\mathbf{f} = \{0 \quad 0 \quad 0 \quad 0 \quad 0 \quad 0 \quad f_1 \quad f_2 \quad f_3 \quad f_4\}^{\mathrm{T}} \tag{28}$$

The negative sign in Eq. (26) represents the fact that the forces are defined as positive when acting upward on the wheelsets.

The dynamic equation for a simply supported bridge using the Euler beam model can be written as

$$EI\frac{\partial^4 y}{\partial x^4} + c_b\frac{\partial y}{\partial t} + m\frac{\partial^2 y}{\partial t^2} = \sum_{i=1}^{4}\left(f_i + \frac{M\mathrm{g}}{4}\right)\delta(x - vt - d_i) \tag{29}$$

in which $y(x,t)$ is the vertical displacement of the bridge; $M = m_b + 2m_t + 4m_w$ is the total mass of the vehicle; v is the vehicle speed, and d_i is the distance between the i-th wheelset and the fourth wheelset.

The wheel-rail contact model is an essential element for analyzing the dynamic performance of the entire system. In general, the contact stiffness between the wheel

and rail can be approximated by a nonlinear Hertz contact spring. However, the proposed frequency-domain method does not hold for a system with a nonlinear element since the superposition principle is violated. It is found that, under a large static contact load, the nonlinear effect on wheel-rail interaction becomes insignificant [36]. In such cases, the nonlinear wheel-rail contact spring can be approximated by a linear one. Therefore, in this study, only the linearized vertical contact spring is considered, and other factors such as the tangential contact and the creep force are not included here. The interaction forces in vector (28) can be then determined by

$$f_i = k_{\mathrm{c}}\left(v_{wi} - y|_{x=vt+d_i} - r|_{x=vt+d_i}\right) + c_{\mathrm{c}}\left(\dot{v}_{wi} - \dot{y}|_{x=vt+d_i} - \dot{r}|_{x=vt+d_i}\right) \quad (30)$$

in which $r(x)$ is the track irregularity under the contact point.

Only vertical track irregularities are considered in this study. These are expressed by the US FRA vertical alignment irregularity PSD function $S_r(\Omega)$ [37]

$$S_r(\Omega) = \frac{kA_r\Omega_c^2}{\Omega^2(\Omega^2 + \Omega_c^2)} \quad (31)$$

where Ω represents the spatial angular frequency of track irregularities; k represents the safety factor, which ranges from 0.25 to 1.0; A_{r} represents the roughness constant; and Ω_c represents the cutoff spatial angular frequency. The class 6 track irregularity spectrum between 1 m and 100 m is used in this study for illustration purposes with $k = 1$, $A_r = 0.0339\ \mathrm{cm}^2 \cdot \mathrm{rad/m}$, and $\Omega_c = 0.8245\ \mathrm{rad/m}$.

3.2 Time-dependent FRFs of coupled system

With the application of the modal-superposition method, the geometric displacement coordinates of each span of the bridge can be transformed to the modal-amplitude coordinates, and the original equation can be decoupled as

$$\ddot{A}_n + 2\xi_n\omega_n\dot{A}_n + \omega_n^2 A_n = \frac{2}{ml}\sum_{i=1}^{4}\left(f_i + \frac{M\mathrm{g}}{4}\right)\phi_n(vt + d_i) \quad (32)$$

due to the modal orthogonality condition, in which $A_n(t)$ is the n-th modal coordinate; $\phi_n(x) = \sin(n\pi x/l)$ is the n-th mode shape of a simply supported beam; $\xi_n = c_b/(2m\omega_n)$ is the n-th modal damping ratio, and $\omega_n = (n^2\pi^2/l^2)\sqrt{EI/m}$ is the n-th modal circular frequency.

When the first N modes of the bridge are of interest, the equivalent LTV system for Eq. (26) and Eq. (32) can be established as

$$\mathbf{L}(p;t)\begin{bmatrix}\mathbf{u}_v\\ A_1\\ A_2\\ \vdots\\ A_N\end{bmatrix}=\mathbf{K}(p;t)\begin{bmatrix}\dfrac{M\mathrm{g}}{4}\\ r(vt+d_1)\\ r(vt+d_2)\\ r(vt+d_3)\\ r(vt+d_4)\end{bmatrix} \tag{33}$$

in which $\mathbf{L}(p;t)$ and $\mathbf{K}(p;t)$ are given in Appendix A.

Note that a transition in the state of the LTV system will take place when each wheelset exits one span and moves into another; also, the vehicle leaving the bridge and moving into the adjacent roadway signifies a transition from an LTV system to an LTI one. In theory, the dynamic equation for each state should be derived and solved separately with the boundary values being continuous at the transition. This leads to obvious complexity in dealing with the calculation using the proposed method.

Nevertheless, these dynamic equations for different states can be reduced to a unified one by simply replacing the mode shape $\phi_n(x)$ with piecewise continuous functions $\phi_{n,s}(x)$

$$\phi_{n,s}(x)=\begin{cases}0 & x<(s-1)l\\ \sin\left[\dfrac{n\pi(x-sl+l)}{l}\right] & (s-1)l\le x<sl\\ 0 & x\ge sl\end{cases} \tag{34}$$

and its derivative $\phi_n'(x)$ with $\phi_{n,s}'(x)$

$$\phi_{n,s}'(x)=\begin{cases}0 & x<(s-1)l\\ \dfrac{n\pi}{l}\cos\left[\dfrac{n\pi(x-sl+l)}{l}\right] & (s-1)l\le x<sl\\ 0 & x\ge sl\end{cases} \tag{35}$$

in which $\phi_{n,s}(x)$ represents the n-th mode shape of the s-th span of the multi-span bridge, with the modal circular frequency $\omega_{n,s}=\omega_n$, as shown in Fig. 3 by taking a three-span bridge as an example.

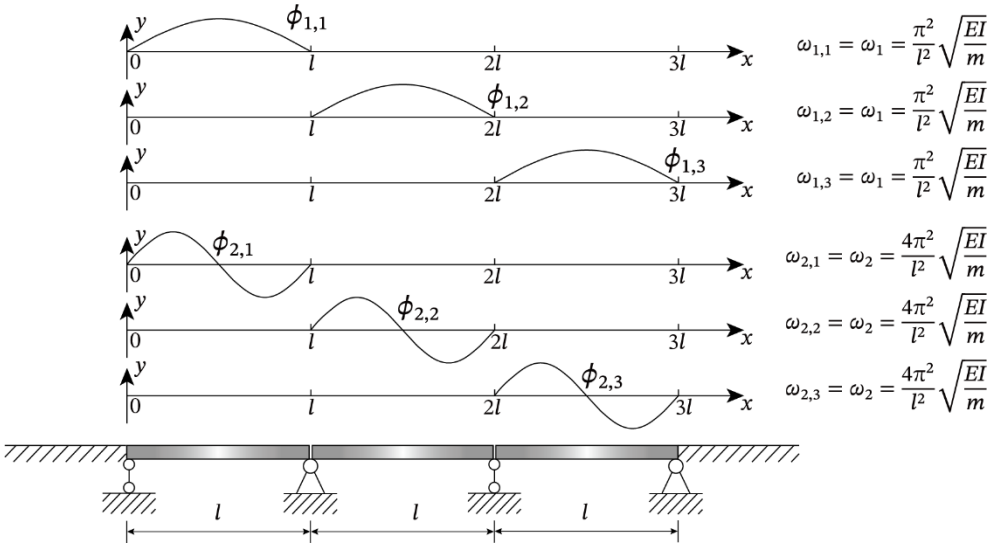

(a)

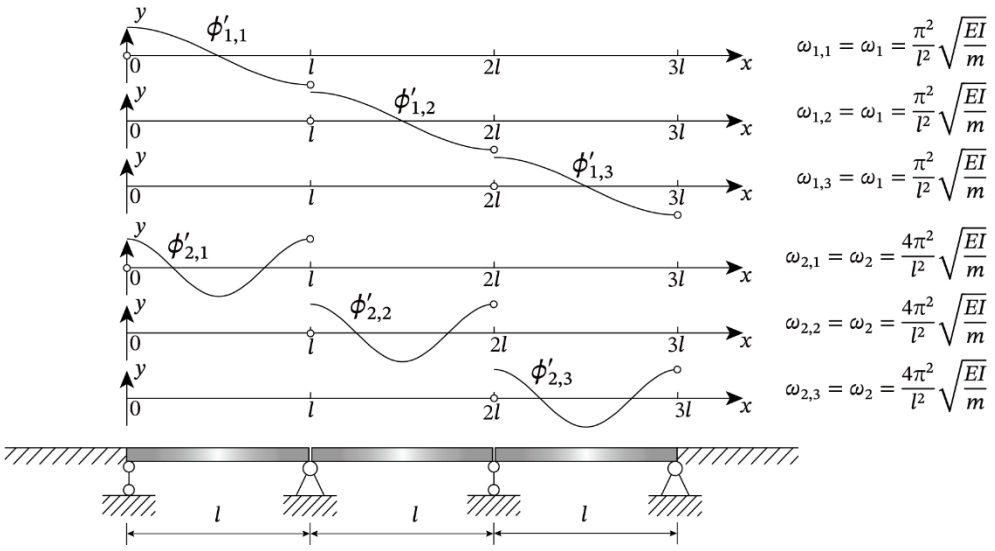

(b)

Fig. 3. Piecewise functions describing the mode shapes and their derivatives for a three-span simply supported bridge: (a) $\phi_{n,s}(x)$; (b) $\phi'_{n,s}(x)$.

In this case, at the original transition in the system state the coefficients of the differential equation for the LTV system become nonanalytic. From a mathematical point of view, the unified equation (modified Eq. (33)) is still solvable since its coefficients are continuous (the discontinuous function $\phi'_{n,s}$ always appears as a continuous product term $\phi_{n,s}\phi'_{n,s}$). Therefore, the whole process of the vehicle crossing each bridge span and moving onto the roadway can be directly solved as if the process had no transitions.

By using Eq. (13), the governing equations of the time-dependent FRFs of the unified LTV system can be obtained as

$$\boldsymbol{\alpha}_2(\mathrm{j}\omega;t)\frac{\mathrm{d}^2\mathbf{H}}{\mathrm{d}t^2}+\boldsymbol{\alpha}_1(\mathrm{j}\omega;t)\frac{\mathrm{d}\mathbf{H}}{\mathrm{d}t}+\mathbf{L}(\mathrm{j}\omega;t)\mathbf{H}=\mathbf{K}(\mathrm{j}\omega;t) \tag{36}$$

in which $\boldsymbol{\alpha}_2(\mathrm{j}\omega;t)$ and $\boldsymbol{\alpha}_1(\mathrm{j}\omega;t)$ are given in Appendix B. Meanwhile, the time-dependent FRFs for displacements $\mathbf{H}_d(\mathrm{j}\omega,t)$, velocities $\mathbf{H}_v(\mathrm{j}\omega,t)$ and accelerations $\mathbf{H}_a(\mathrm{j}\omega,t)$ of the vehicle-bridge coupled system are given in Appendix B.

3.3 Response EPSDs

Substituting $\mathbf{H}_d(\mathrm{j}\omega,t)$, $\mathbf{H}_v(\mathrm{j}\omega,t)$ and $\mathbf{H}_a(\mathrm{j}\omega,t)$ into Eq. (23), the evolutionary spectral density matrix for the steady-state displacement response $\mathbf{S}_d(\omega,t)$, the velocity response $\mathbf{S}_v(\omega,t)$ and the acceleration response $\mathbf{S}_a(\omega,t)$ are obtained as

$$\mathbf{S}_d(\omega,t)=\mathbf{H}_d^*(\mathrm{j}\omega,t)\begin{bmatrix}0 & 0\\ 0 & \mathbf{S}_r(\omega)\end{bmatrix}\mathbf{H}_d^{\mathrm{T}}(\mathrm{j}\omega,t) \tag{37}$$

$$\mathbf{S}_v(\omega,t)=\mathbf{H}_v^*(\mathrm{j}\omega,t)\begin{bmatrix}0 & 0\\ 0 & \mathbf{S}_r(\omega)\end{bmatrix}\mathbf{H}_v^{\mathrm{T}}(\mathrm{j}\omega,t) \tag{38}$$

$$\mathbf{S}_a(\omega,t)=\mathbf{H}_a^*(\mathrm{j}\omega,t)\begin{bmatrix}0 & 0\\ 0 & \mathbf{S}_r(\omega)\end{bmatrix}\mathbf{H}_a^{\mathrm{T}}(\mathrm{j}\omega,t) \tag{39}$$

where $\mathbf{S}_r(\omega)$ is defined as the spectral density matrix for the irregularities at the contact points given by

$$\mathbf{S}_r(\omega)=\lim_{T\to\infty}\frac{\mathbf{R}^*\mathbf{R}^{\mathrm{T}}}{2T}=\boldsymbol{\mathcal{B}}(\omega,v)\frac{1}{v}S_r\left(\frac{\omega}{v}\right) \tag{40}$$

in which $S_r(\Omega)$ is the spatial-PSD function of track irregularities given in Eq. (31). $\boldsymbol{\mathcal{B}}(\omega,v)$ is a phase-lag matrix, describing relationships of time delay among the excitations. The use of the phase-lag matrix allows different types of excitations to be represented. For example, at low frequencies, excitations at the four wheelsets can be regarded as strictly correlated, and $\boldsymbol{\mathcal{B}}(\omega,v)$ can be expressed as [21]

$$\boldsymbol{\mathcal{B}}(\omega,v)=\begin{bmatrix}1 & \mathrm{e}^{-\mathrm{i}\frac{\omega}{v}2b} & \mathrm{e}^{-\mathrm{i}\frac{\omega}{v}2(b+a)} & \mathrm{e}^{-\mathrm{i}\frac{\omega}{v}2(2b+a)}\\ \mathrm{e}^{\mathrm{i}\frac{\omega}{v}2b} & 1 & \mathrm{e}^{-\mathrm{i}\frac{\omega}{v}2a} & \mathrm{e}^{-\mathrm{i}\frac{\omega}{v}2(b+a)}\\ \mathrm{e}^{\mathrm{i}\frac{\omega}{v}2(b+a)} & \mathrm{e}^{\mathrm{i}\frac{\omega}{v}2a} & 1 & \mathrm{e}^{-\mathrm{i}\frac{\omega}{v}2b}\\ \mathrm{e}^{\mathrm{i}\frac{\omega}{v}2(2b+a)} & \mathrm{e}^{\mathrm{i}\frac{\omega}{v}2(b+a)} & \mathrm{e}^{\mathrm{i}\frac{\omega}{v}2b} & 1\end{bmatrix} \tag{41}$$

Meanwhile, the time-varying RMS for the displacement response $\boldsymbol{\sigma}_d(t)$, the velocity response $\boldsymbol{\sigma}_v(t)$ and the acceleration response $\boldsymbol{\sigma}_a(t)$ of the system can be determined by using Eq. (24), and the time-varying mean of the steady-state response can be obtained based on Eq. (25).

For the sake of clarity, the analytical formula derived in this study only correspond to a simply supported bridge with three spans. When considering any general bridge, the mode shape functions $\phi_n(x)$ and mode frequencies ω_n should be adjusted to match the results of a modal analysis. For instance, a simply supported Euler beam on an elastic foundation can be used to represent approximately cable-stayed bridges and suspension bridges, leading to different modal frequencies [38]. However, the presented methodology is not substantially changed if different modal parameters are considered.

4 Case study

The investigation is based on a high-speed railway vehicle running on a three-span simply supported bridge at $60\ \mathrm{m/s}$. Tables 1 and 2 list the main parameters for the bridge and the vehicle with their values given by Wu and Yang [39]. Only the first five modes of each bridge span are considered, which have natural frequencies in the range from 4.88 Hz to 122 Hz, which is sufficient to cover the dominant frequencies of the system response. Before crossing the bridge, the vehicle is assumed to move on the track irregularities on a rigid roadway with sufficient length until reaching a stationary state; the bridge is initially at rest.

Table 1. Parameters for a railway bridge based on Euler beam model [39].

Parameter	Units	Value	Parameter	Units	Value

EI	MNm^2	2.459×10^5	m	kg/m	3.14×10^4
ξ	/	0.01	l	m	30

Table 2. Parameters for a high-speed railway vehicle [39].

Parameter	Unit	Value	Parameter	Unit	Value
m_b	kg	41750	k_1	N/m	1.18×10^6
J_b	$\mathrm{kg \cdot m}^2$	2.08×10^6	c_1	$\mathrm{N \cdot s/m}$	3.92×10^4
m_t	kg	3040	k_2	N/m	5.3×10^5
J_t	$\mathrm{kg \cdot m}^2$	3930	c_2	$\mathrm{N \cdot s/m}$	9.02×10^4
m_w	kg	1780	k_c	N/m	1.5×10^8
a	m	8.75	c_c	$\mathrm{N \cdot s/m}$	1.8×10^5
b	m	1.25			

4.1 Validations

The proposed spectral analysis method is first justified by comparing its results with those obtained by using the MCM. The irregularity samples for the MCM are generated from the US FRA class 6 spectrum given by Eq. (34). A fourth order Runge-Kutta method is used to calculate the time history responses, with integration step $\Delta t = 0.001$ s. Considering the convergence speed for estimating different statistical characteristics, both 1000 and 5000 samples are used in the Monte Carlo simulation. The RMS responses obtained by the proposed method are calculated by integrating the response EPSD over 1000 frequency points.

Fig. 4 shows the mean values at each instant of time for the vertical displacement and acceleration of the car body and the midspan of the first bridge span, as well as the first wheel-rail contact force, given by Eq. (25) and by the MCM with 1000 and 5000 samples. The results are calculated from 0 s to 2 s, in which the first wheelset arrives at the first span at $t = 0$ s and leaves the third span at $t = 1.5$ s before continuing to run on the rigid roadway with track irregularities. The vertical lines represent the transitions at which the first wheel leaves the first span at $t = 0.5$ s, and the last wheel leaves the first span at $t = 0.83$ s.

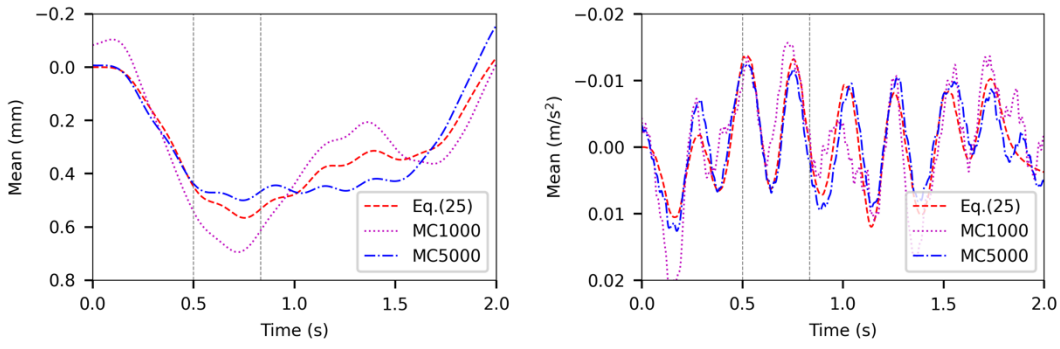

(a) (b)

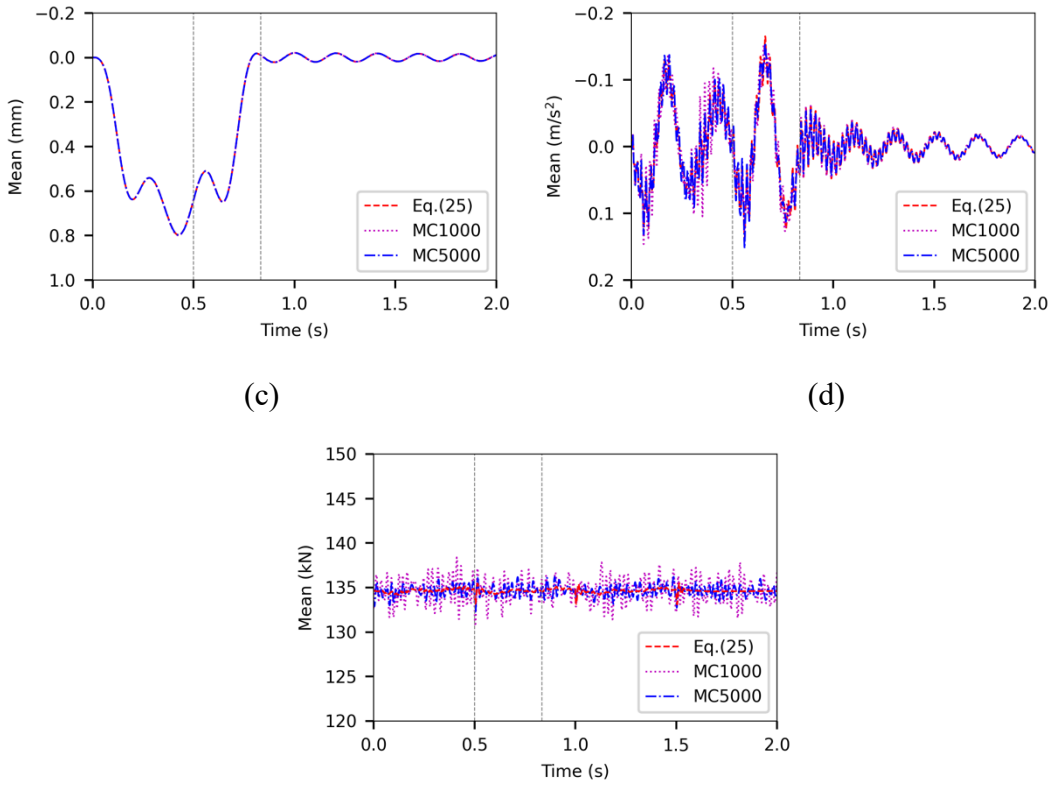

Fig. 4. Mean values of the response for the vehicle-bridge coupled system with the vehicle running on track irregularities at $60\ \mathrm{m/s}$ obtained by Eq. (25) and the MCM with 1000 and 5000 samples: (a) vertical displacement of the car body; (b) vertical acceleration of the car body; (c) displacement of the bridge midspan; (d) acceleration of the bridge midspan; (e) first wheel-rail contact force.

In general, the mean responses calculated by using Eq. (25) and the MCM with 5000 samples are in good agreement. However, the MCM converges very slowly for the mean responses of the car body. As proved in Section 2.4, the mean response is time-varying due to the moving mass effect. Therefore, to ensure a good accuracy, the time-domain method regarding the track as smooth can be adopted instead of the MCM. As shown in Fig. 4, the mean displacement responses start at zero and reach their maximum when the first wheel arrives at around the end of the first span ($t = 0.5$ s). The mean result for the contact force stabilizes at around 134.6 kN, i.e., the axle load, with only slight fluctuations at the moment of the first wheel crossing the bridge joints ($t = 0.5\ \mathrm{s}, 1.0\ \mathrm{s}, 1.5\ \mathrm{s}$).

The time-varying RMS of the vertical displacement and acceleration of the car body and the midspan of the first bridge span, as well as the first wheel-rail contact force, are shown in Fig. 5, obtained by the proposed method with the 2nd-order perturbation method and by the MCM with 1000 and 5000 samples.

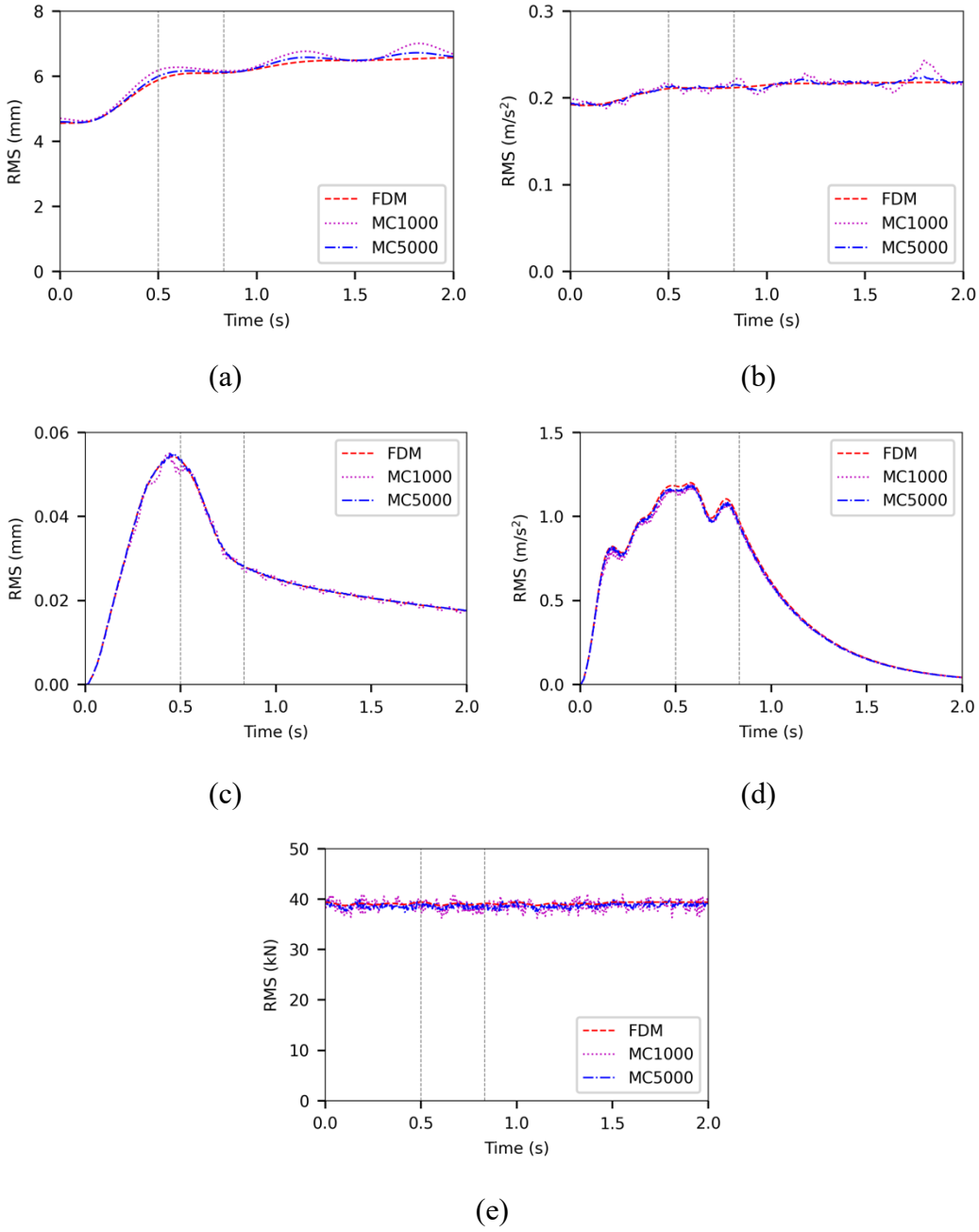

Fig. 5. Time-varying RMS of the response for the vehicle-bridge coupled system with the vehicle running on track irregularities at 60 m/s: (a) vertical displacement of the car body; (b) vertical acceleration of the car body; (c) displacement of the first bridge midspan; (d) acceleration of the first bridge midspan; (e) first wheel-rail contact force.

The time-varying RMS calculated by the proposed method and the MCM are in very good agreement, which shows the reliability of the proposed method. Note that 1000 samples have already provided an adequate approximation to the RMS of the vehicle response, while 5000 samples are not enough for the mean responses as shown in Fig. 4. According to the theory of probability and statistics [40], to achieve a 95% confidence interval for the estimation with a relative error less than 5 %, the minimum

number of the samples N should satisfy $N \geq \left(\frac{1.96\sigma}{0.05\mu}\right)^2$ for estimating the mean, and $\sqrt{\frac{\chi^2_{0.025,N-1}}{N-1}} \geq 0.95$ together with $\sqrt{\frac{\chi^2_{0.975,N-1}}{N-1}} \leq 1.05$ for the standard deviation, in which $\chi^2_{p,N-1}$ is the p-th percentile of a chi-squared distribution with $N-1$ DOFs. It is seen that the RMS of the car body response is almost 10 times larger than its mean, leading to a minimum of 150,000 samples for obtaining an accurate mean response. In contrast, the minimum sample number for estimating the RMS is calculated as 768, and it was further verified that this can ensure a generally good accuracy as expected. Moreover, the computational efficiency of the proposed method is much higher than that of the MCM. In this study, an Intel Core i5 4-Core computer with main frequency 2.3 GHz and 16 GB RAM is used. The computation time by the proposed method is about 0.46 h, whereas the time taken by the MCM with 1000 samples is about 4.5 h (without parallel computing).

The RMS results for the vehicle and the contact force stabilize at around stationary responses with slight fluctuations. In contrast, the bridge response does not tend to a stable limit. Both displacement and acceleration RMS values start at zero and gradually increase until the vehicle reaches around the end of the first span, after which, the amplitude gradually reduces due to its damped free vibration and will finally reach zero after a long enough time. The RMS of the vehicle displacement is much larger than that of the bridge, whereas the RMS of acceleration of the bridge is much larger than that of the vehicle, yet the mean values of each in Fig. 4 are quite similar.

4.2 Discussions on response spectrums

Fig. 6 gives the EPSD of the vertical displacements and accelerations of the car body and the midspan of the first bridge span, obtained by the proposed spectral analysis method with the 2nd-order perturbation method. The EPSD at frequencies from 0.6 Hz to 60 Hz are calculated, corresponding to the cut-off wavelengths at 1 m and 100 m for track irregularities with the vehicle speed at 60 m/s. Only the results below 6 Hz are shown for the car body, because the response of the car body is relatively small at higher frequencies, whereas the frequency range for the bridge response is extended to 60 Hz. Besides, the EPSDs for the system response at $t = 0.25$ s, $t = 0.5$ s and $t = 1.5$ s, that correspond to the instants when the first wheel passes the midspan, the end of the first span and the end of the third span, are shown in Fig. 7.

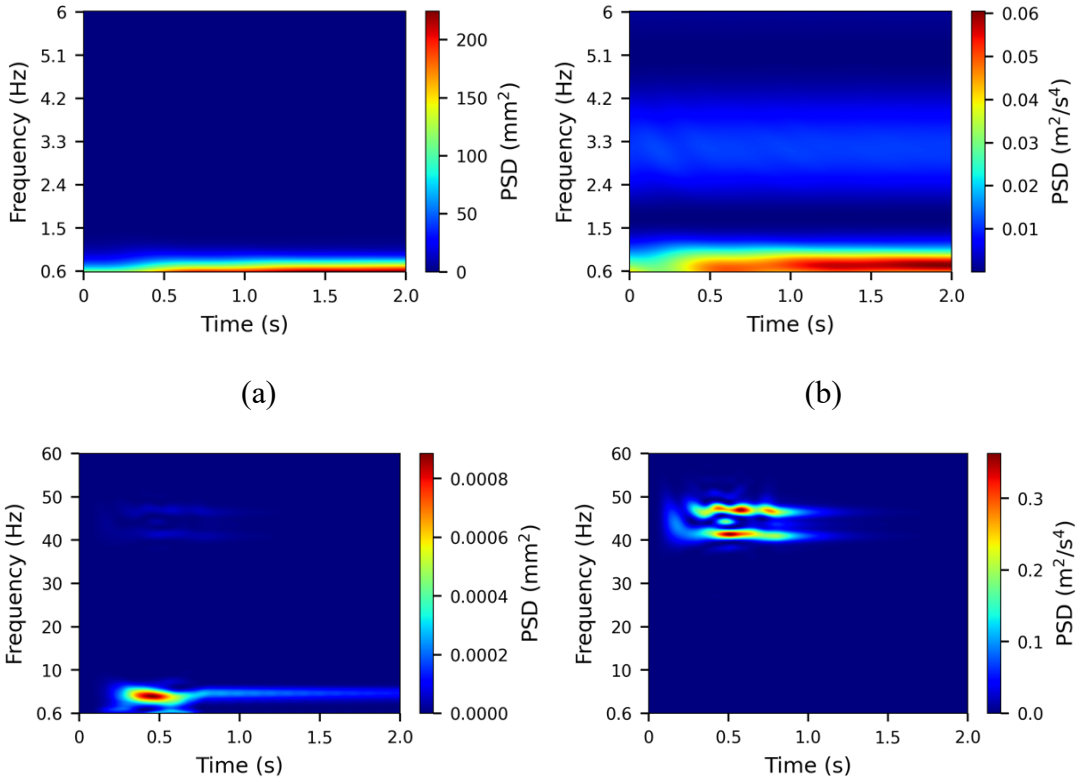

Fig. 6. EPSD of the responses for the vehicle-bridge coupled system: (a) vertical displacement of the car body; (b) vertical acceleration of the car body; (c) displacement of the first bridge midspan; (d) acceleration of the first bridge midspan.

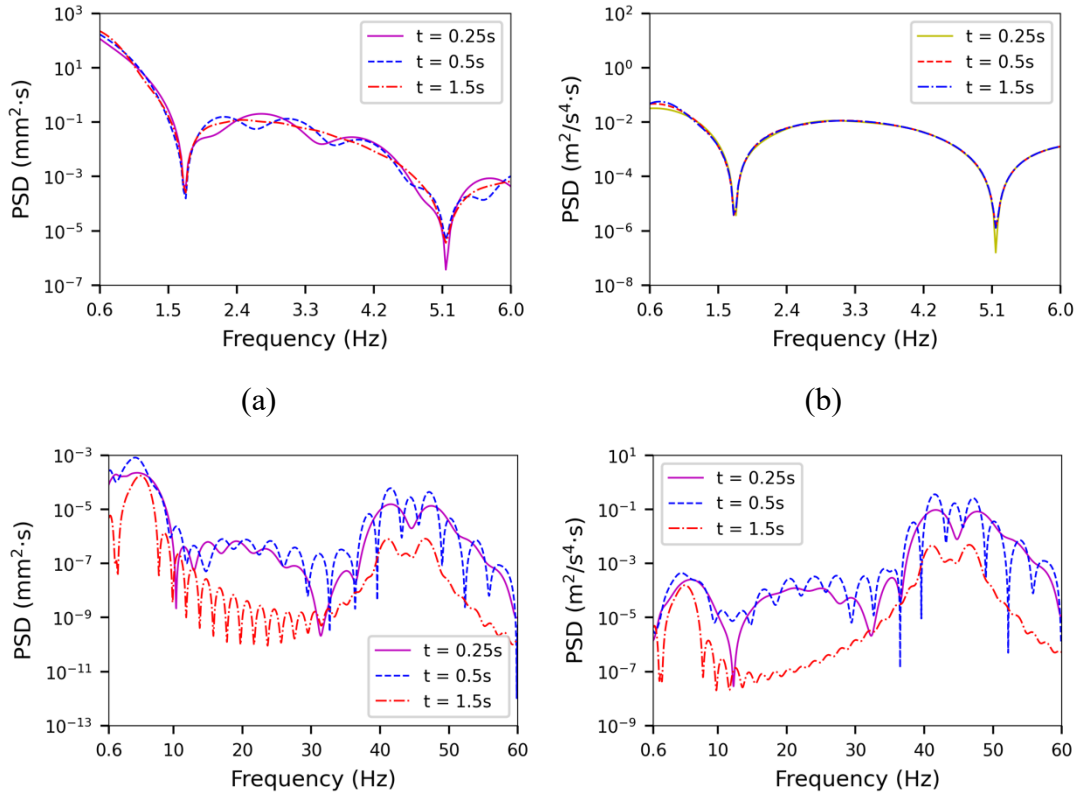

(c) (d)

Fig. 7. EPSDs of the system response at $t = 0.25$ s, $t = 0.5$ s and $t = 1.5$ s: (a) vertical displacement of the car body; (b) vertical acceleration of the car body; (c) displacement of the first bridge midspan; (d) acceleration of the first bridge midspan.

The EPSD results show again that the magnitudes are quite different between the displacement responses of the car body and the bridge, as discussed for the RMS results. It is seen from Fig. 6 (a) and (b) that the EPSD for the car body rapidly tends to a steady state and varies only slightly with time. This is also verified in Fig. 7 (a) and (b) as the PSDs at different times have only slight deviations from each other. This indicates that the bridge vibration has little influence on the stochastic response of the vehicle apart from the time-varying characteristics of the mean response. In other words, the vibration of the vehicle can be regarded as a stationary process, so the non-stationary vibration of the vehicle can be evaluated as if the vehicle was running on a rigid roadway with track irregularities. Note that the troughs in the response PSDs of the car body occur due to the effect of the spatial lag between different wheels, which can also be found in the stationary response of the car body for a vehicle running on a rigid roadway with track irregularities [21].

In contrast, the magnitude of the EPSD for the bridge starts at zero and gradually increases with time until the vehicle reaches the end of the first span, especially at the peak frequencies (see Fig. 6 (c) and (d)), since the response of the bridge takes time to build up, after which the magnitude rapidly decreases to zero due to the damped free vibration of the bridge with random initial values. Moreover, the dominant frequency changes with time, e.g., the dominant frequencies in the acceleration EPSD shift from 41.5 Hz at $t = 0.5$ s to 47.1 Hz at $t = 0.6$ s as shown in Fig. 6 (d), and the peaks gradually become closer to the modal frequencies with time. These results imply that the response of the bridge shows a stronger characteristic of non-stationarity than the vehicle.

Fig. 7 (a) shows that the displacement EPSD of the car body is dominated by low frequency components. This implies that the displacement response is more related to the irregularity PSD distribution and the vibration of the bridge rather than the modal response of the vehicle. The dominant frequency for the acceleration EPSD (Fig. 6 (b)), however, is close to the natural frequency of the bounce mode of the car body on the secondary suspension, which is around 0.85 Hz. The peaks in the EPSD for the bridge (Fig. 6 (c) and (d)) correspond to its modal frequencies. Moreover, the dominant frequencies in the acceleration EPSD of the bridge are higher than those in the displacement EPSD, mainly due to the factor of ω^4 in the relationship between them. This means that, to evaluate the acceleration response of the bridge, the contribution of

short-wavelength components of track irregularities should be considered. In contrast, the long-wavelength components are responsible for the car body response and bridge displacement. Notice that the natural frequency of the wheel bouncing on the equivalent contact spring is around 46 Hz. Therefore, to obtain reliable wheel responses and wheel-rail contact forces, short-wavelength irregularities should be included.

4.3 Extreme values of the response

The extreme values of the response are usually of particular interest for practical engineering applications. However, in conventional analysis, one should select the maximum response from dozens or hundreds of response samples, i.e., using Monte Carlo simulations, to give an estimation of the extreme values. It has been already shown that the mean value and the standard deviation of the response can easily be calculated by using the proposed spectral analysis method. Note that the stochastic response still retains Gaussian characteristics despite the fact that it is non-stationary [41], so the 3σ rule that corresponds to a 99.73 % confidence interval, i.e., $\mu \pm 3\sigma$, can be adopted to estimate the boundaries of the response [1]. This will be more reliable and efficient than the conventional method based on Monte Carlo simulations.

Fig. 8 gives the lower and the upper bounds for the vertical displacements and the accelerations of the car body and the midspan of the first bridge span obtained by the 3σ rule for track irregularities of class 6. In each case three response samples from the Monte Carlo simulation results are shown for comparison.

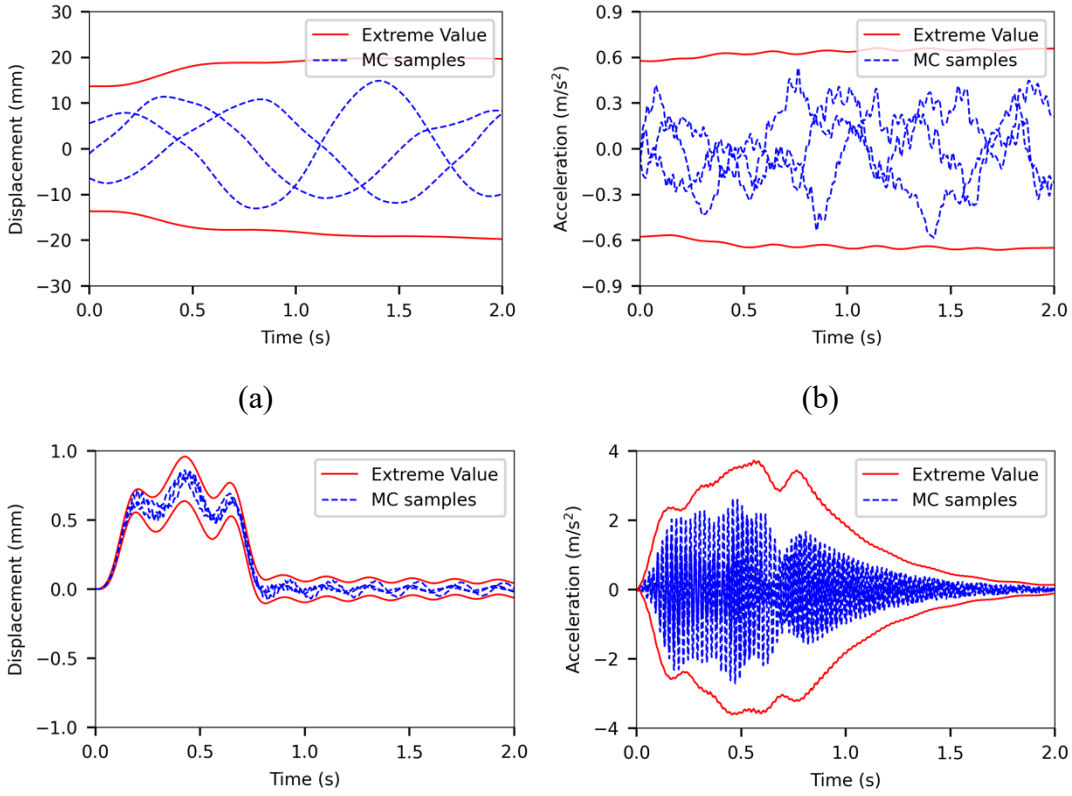

(c) (d)

Fig. 8. Lower and the upper bounds of the response for the vehicle-bridge coupled system for track irregularities of class 6: (a) displacement of the car body; (b) acceleration of the car body; (c) displacement of the bridge midspan; (d) acceleration of the bridge midspan.

Firstly, Fig. 8 shows that the Monte Carlo simulation samples are all located between the bounds, and by evaluating 5000 samples it was further verified that they are all located in this area as expected for a $99.73\ \%$ confidence interval. This shows the reliability of the 3σ rule for the extreme value analysis of the non-stationary vibration. A higher multiple of σ could be used if a greater confidence interval is required. Moreover, it is seen that the upper and lower bounds differ widely from each other for the car body and the bridge acceleration, whereas they are very close to each other for the bridge displacement.

To investigate further the influence of track irregularities on extreme responses of the vehicle and the bridge, the results for three different amplitudes of track irregularities (track irregularity of class 4 with $A_r = 0.5376\ \mathrm{cm}^2 \cdot \mathrm{rad/m}$, class 5 with $A_r = 0.2095\ \mathrm{cm}^2 \cdot \mathrm{rad/m}$ and class 6 with $A_r = 0.0339\ \mathrm{cm}^2 \cdot \mathrm{rad/m}$) are shown in Fig. 9. Note that the results for class 4 and 5 can be easily obtained based on the previous results for track class 6 since the EPSD (or time-varying variance) of the response is proportional to the PSD of track irregularities as given in Eq. (37)-(39), and thus proportional to A_r as well.

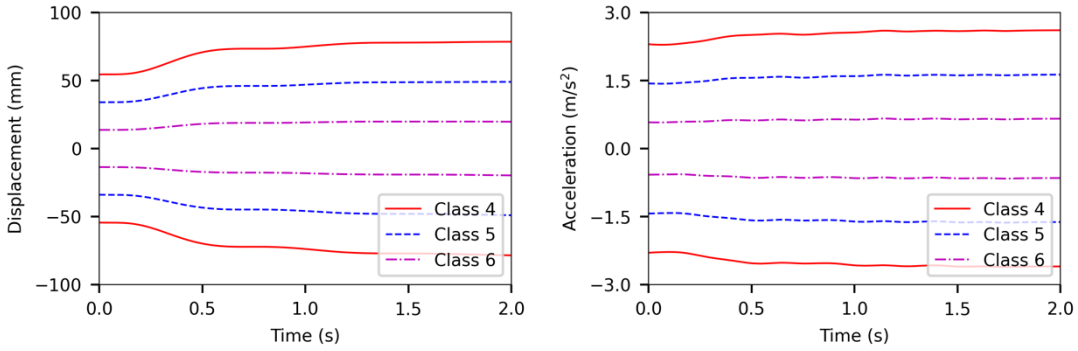

(a) (b)

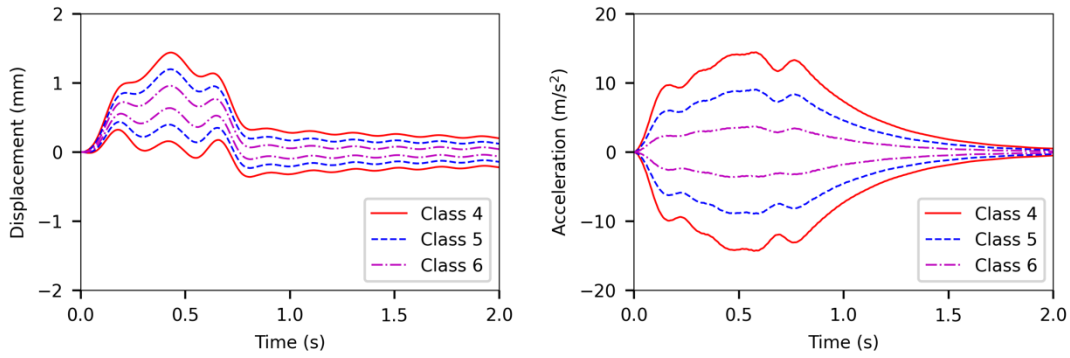

(c) (d)

Fig. 9. Lower and the upper bounds of the response for the vehicle-bridge coupled system for track irregularities of class 4, 5 and 6: (a) displacement of the car body; (b) acceleration of the car body; (c) displacement of the bridge midspan; (d) acceleration of the bridge midspan.

With the increase of the amplitude of track irregularities, the bounds for each response become wider. The lower and the upper bounds remain symmetric with each other for both the vehicle responses and the bridge accelerations. In contrast, the bounds for the bridge displacement are relatively narrow and skewed to the positive side, which resemble the mean response as shown in Fig. 4 (c) (downward positive in Fig. 4). This means that the RMS values play a dominant role for the bounds of the vehicle response and the bridge accelerations, whereas the bounds for the displacement response of the bridge are dominated by the mean values. The results show that the track irregularities have a significant effect on the vibration of the vehicle, while they are less significant for the bridge displacement, which are dominated by the moving mass effect.

5 Conclusions

This study has investigated the stochastic vibration of a high-speed railway vehicle running on a three-span simply supported bridge subjected to track irregularities. Due to the movement of the vehicle, the coupled system becomes time dependent, and the responses are non-stationary even if the track irregularities are assumed to be stationary. Based on Priestley's Evolutionary Spectra theory, a spectral analysis method has been presented to calculate the evolutionary spectra of the response. The FRFs used in this method are also time dependent and can be determined by a set of linear differential equations. By extending the mode shapes of each span to cover the full structure, the transitions occurring when the wheels of the vehicle cross the joints between each bridge span and between the bridge and the adjacent roadway can be considered and the whole process can be directly solved without separating each state.

The proposed spectral analysis method is validated by comparisons with Monte Carlo simulations. In the Monte Carlo method, intensive simulations are needed due to

the non-stationary characteristics of the response, especially for the vehicle response. The results show that the non-stationary response can be regarded as the summation of a deterministic time-varying mean which is due to the moving mass effect, and a zero-mean non-stationary component that can be characterized by the EPSD. The magnitudes of the RMS and EPSD for the vehicle displacement vary little with time, and are much larger than those of the bridge, implying that the non-stationary vibration of the vehicle can be regarded as a stationary process. In contrast, the results for the bridge vary a lot with time and present a stronger characteristic of non-stationarity.

The 3σ rule can be adopted to estimate the extreme values of the non-stationary responses of the coupled system directly from the proposed method. The results show that the RMS values have played a dominant role for the extreme values of the vehicle response and the bridge accelerations. In contrast, the extreme values for the bridge displacement are dominated by the mean values. This means that the track irregularities are more relevant to the vibration of the vehicle and the bridge acceleration, whereas the bridge displacement is dominated by the moving mass effect.

The present method is a spectral analysis method focusing on the second-order statistics of the response, which is limited to linear systems with random excitations but without random system parameters. In future work, the proposed method can be extended to evaluate the system with small parameter uncertainty using the random perturbation method and also including a three-dimensional train-bridge system with linearized wheel-rail contact model.

Acknowledgements

The study was supported by the National Natural Science Foundation of China (grant numbers 51878501, and 51778495 and 51978527) and the China Scholarship Council (No.202106260170).

Appendix A. Coefficients of the LTV system

$$\mathbf{m}_v = \mathrm{diag}[m_b \quad J_b \quad m_t \quad J_t \quad m_t \quad J_t \quad m_w \quad m_w \quad m_w \quad m_w] \tag{A1}$$

$$\mathbf{c}_v = \begin{bmatrix}
2c_2 & & -c_2 & & -c_2 & & & & & \\
 & 2a^2c_2 & -ac_2 & & ac_2 & & & & & \\
-c_2 & -ac_2 & c_2+2c_1 & & & & -c_1 & -c_1 & & \\
 & & & 2b^2c_1 & & & -bc_1 & bc_1 & & \\
-c_2 & ac_2 & & & c_2+2c_1 & & & & -c_1 & -c_1 \\
 & & & & & 2b^2c_1 & & & -bc_1 & bc_1 \\
 & & -c_1 & -bc_1 & & & c_1 & & & \\
 & & -c_1 & bc_1 & & & & c_1 & & \\
 & & & & -c_1 & -bc_1 & & & c_1 & \\
 & & & & -c_1 & bc_1 & & & & c_1
\end{bmatrix} \tag{A2}$$

$$\mathbf{k}_v = \begin{bmatrix} 2k_2 & & -k_2 & & -k_2 & & & & & \\ & 2a^2k_2 & -ak_2 & & ak_2 & & & & & \\ -k_2 & -ak_2 & k_2+2k_1 & & & & -k_1 & -k_1 & & \\ & & & 2b^2k_1 & & & -bk_1 & bk_1 & & \\ -k_2 & ak_2 & & & k_2+2k_1 & & & & -k_1 & -k_1 \\ & & & & & 2b^2k_1 & & & -bk_1 & bk_1 \\ & & -k_1 & -bk_1 & & & k_1 & & & \\ & & -k_1 & bk_1 & & & & k_1 & & \\ & & & & -k_1 & -bk_1 & & & k_1 & \\ & & & & -k_1 & bk_1 & & & & k_1 \end{bmatrix} \quad \text{(A3)}$$

$$\mathbf{L}(p;t) = \begin{bmatrix} \mathbf{m}_v & \mathbf{0} \\ \mathbf{0} & \text{diag}\left\{\frac{ml}{2} \quad \cdots \quad \frac{ml}{2}\right\} \end{bmatrix} \times p^2$$
$$+ \left\{ \begin{bmatrix} \mathbf{c}_v & \mathbf{0} \\ \mathbf{0} & ml\text{diag}\{\xi_1\omega_1 \quad \cdots \quad \xi_N\omega_N\} \end{bmatrix} + c_c \sum_{i=1}^{4} \boldsymbol{\Psi}_i \boldsymbol{\Psi}_i^{\mathrm{T}} \right\} \times p \quad \text{(A4)}$$
$$+ \begin{bmatrix} \mathbf{k}_v & \mathbf{0} \\ \mathbf{0} & \frac{ml}{2}\text{diag}\{\omega_1^2 \quad \cdots \quad \omega_N^2\} \end{bmatrix} + k_c \sum_{i=1}^{4} \boldsymbol{\Psi}_i \boldsymbol{\Psi}_i^{\mathrm{T}} + vc_c \sum_{i=1}^{4} \boldsymbol{\Psi}_i \boldsymbol{\Psi}_i'^{\mathrm{T}}$$

$$\mathbf{K}(p;t) = [\mathbf{0} \quad -c_c\boldsymbol{\Psi}_1 \quad -c_c\boldsymbol{\Psi}_2 \quad -c_c\boldsymbol{\Psi}_3 \quad -c_c\boldsymbol{\Psi}_4] \times p$$
$$+ \begin{bmatrix} 0 & & & & \\ \vdots & & & & \\ 0 & & & & \\ \sum_{i=1}^{4} \phi_1(vt+d_i) & -k_c\boldsymbol{\Psi}_1 & -k_c\boldsymbol{\Psi}_2 & -k_c\boldsymbol{\Psi}_3 & -k_c\boldsymbol{\Psi}_4 \\ \vdots & & & & \\ \sum_{i=1}^{4} \phi_N(vt+d_i) & & & & \end{bmatrix} \quad \text{(A5)}$$

in which $\boldsymbol{\Psi}_i$ represents the vector of the mode shape $\phi_n(x)$ where $x = vt + d_i$ and -1 at the $6+i$-th row corresponding to the i-th wheelsets

$$\boldsymbol{\Psi}_i = \begin{bmatrix} 0 \\ \vdots \\ 0 \\ -1 \\ 0 \\ \vdots \\ 0 \\ \phi_1(vt+d_i) \\ \vdots \\ \phi_N(vt+d_i) \end{bmatrix} \begin{matrix} 1 \\ \vdots \\ 5+i \\ 6+i \\ 7+i \\ \vdots \\ 10 \\ 11 \\ \vdots \\ 10+N \end{matrix} \quad \text{(A6)}$$

Appendix B. Coefficients corresponding to time-dependent FRFs

$$\boldsymbol{\alpha}_2(\mathrm{j}\omega;t)=\begin{bmatrix}\mathbf{m}_v & \mathbf{0}\\ \mathbf{0} & \mathrm{diag}\left\{\frac{ml}{2} \quad \cdots \quad \frac{ml}{2}\right\}\end{bmatrix} \tag{B1}$$

$$\begin{aligned}\boldsymbol{\alpha}_1(\mathrm{j}\omega;t)=&\ 2\mathrm{j}\omega\begin{bmatrix}\mathbf{m}_v & \mathbf{0}\\ \mathbf{0} & \mathrm{diag}\left\{\frac{ml}{2} \quad \cdots \quad \frac{ml}{2}\right\}\end{bmatrix}\\ &+\begin{bmatrix}\mathbf{c}_v & \mathbf{0}\\ \mathbf{0} & ml\mathrm{diag}\{\xi_{1,1}\omega_{1,1} \quad \xi_{1,2}\omega_{1,2} \quad \cdots \quad \xi_{N,S}\omega_{N,S}\}\end{bmatrix}+c_c\sum_{i=1}^{4}\boldsymbol{\Psi}_i\boldsymbol{\Psi}_i^{\mathrm{T}}\end{aligned} \tag{B2}$$

in which S is the number of the bridge span and $\boldsymbol{\Psi}_i$ considers the modified mode shape $\phi_{n,s}(x)$

$$\boldsymbol{\Psi}_i=\begin{bmatrix}0\\ \vdots\\ 0\\ -1\\ 0\\ \vdots\\ 0\\ \phi_{1,1}(vt+d_i)\\ \phi_{1,2}(vt+d_i)\\ \vdots\\ \phi_{N,S}(vt+d_i)\end{bmatrix}\begin{matrix}1\\ \vdots\\ 5+i\\ 6+i\\ 7+i\\ \vdots\\ 10\\ 11\\ 12\\ \vdots\\ 10+N\times S\end{matrix} \tag{B3}$$

$$\mathbf{H}_d(\mathrm{j}\omega,t)=\mathbf{T}\mathbf{H}(\mathrm{j}\omega,t) \tag{B4}$$

$$\mathbf{H}_v(\mathrm{j}\omega,t)=\mathbf{T}\left[\dot{\mathbf{H}}(\mathrm{j}\omega,t)+\mathrm{j}\omega\mathbf{H}(\mathrm{j}\omega,t)\right] \tag{B5}$$

$$\mathbf{H}_a(\mathrm{j}\omega,t)=\mathbf{T}\left[\ddot{\mathbf{H}}(\mathrm{j}\omega,t)+2\mathrm{j}\omega\dot{\mathbf{H}}(\mathrm{j}\omega,t)-\omega^2\mathbf{H}(\mathrm{j}\omega,t)\right] \tag{B6}$$

$$\mathbf{T}=\begin{bmatrix}1 & 0 & \cdots & 0 & 0 & 0 & \cdots & 0\\ 0 & 1 & \ddots & \vdots & 0 & 0 & \cdots & 0\\ \vdots & \ddots & \ddots & 0 & \vdots & \vdots & \ddots & \vdots\\ 0 & \cdots & 0 & 1 & 0 & 0 & \cdots & 0\\ 0 & 0 & \cdots & 0 & \phi_{1,1}(x) & \phi_{1,2}(x) & \cdots & \phi_{N,S}(x)\end{bmatrix} \tag{B7}$$

References

[1] F. Lu, J. Lin, D. Kennedy, F.W. Williams, An algorithm to study non-stationary random vibrations of vehicle–bridge systems, Computers & Structures, 87 (2009) 177-185.

[2] Z. Zhang, J. Lin, Y. Zhang, Y. Zhao, W.P. Howson, F.W. Williams, Non-stationary random vibration analysis for train–bridge systems subjected to horizontal earthquakes, Eng. Struct., 32 (2010) 3571-3582.

[3] G. Lombaert, J.P. Conte, Random vibration analysis of dynamic vehicle-bridge interaction due to road unevenness, Journal of engineering mechanics, 138 (2012) 816-825.

[4] L.A. Zadeh, Frequency analysis of variable networks, Proceedings of the IRE, 38 (1950) 291-299.
[5] L.A. Zadeh, The determination of the impulsive response of variable networks, Journal of Applied Physics, 21 (1950) 642-645.
[6] L. Frýba, Non-stationary response of a beam to a moving random force, J. Sound Vibr., 46 (1976) 323-338.
[7] R. Iwankiewicz, P. Śniady, Vibration of a beam under a random stream of moving forces, Journal of Structural Mechanics, 12 (1984) 13-26.
[8] H. Xia, G. De Roeck, H. Zhang, N. Zhang, Dynamic analysis of train–bridge system and its application in steel girder reinforcement, Computers & Structures, 79 (2001) 1851-1860.
[9] W.M. Zhai, Z.L. Han, Z.W. Chen, L. Ling, S.Y. Zhu, Train-track-bridge dynamic interaction: A state-of-the-art review, Veh. Syst. Dyn., 57 (2019) 984-1027.
[10] W. Zhai, H. Xia, C. Cai, M. Gao, X. Li, X. Guo, N. Zhang, K. Wang, High-speed train–track–bridge dynamic interactions–part i: Theoretical model and numerical simulation, International Journal of Rail Transportation, 1 (2013) 3-24.
[11] W. Zhai, C. Cai, Train/track/bridge dynamic interactions: Simulation and applications, Veh. Syst. Dyn., 37 (2002) 653-665.
[12] L. Xu, W. Zhai, A three-dimensional model for train-track-bridge dynamic interactions with hypothesis of wheel-rail rigid contact, Mechanical Systems and Signal Processing, 132 (2019) 471-489.
[13] J.H. Lin, Y.H. Zhang, Y. Zhao, X.F. Xu, G.W. Tang, Seismic random vibration analysis for long span structures, International Conference on Advances in Structural Dynamics (ASD 2000), Hong Kong, Peoples R China, 2000, pp. 931-938.
[14] J. Lin, W. Zhang, F. Williams, Pseudo-excitation algorithm for nonstationary random seismic responses, Eng. Struct., 16 (1994) 270-276.
[15] Z. Zhang, J. Lin, Y. Zhang, W.P. Howson, F.W. Williams, Non-stationary random vibration analysis of three-dimensional train–bridge systems, Veh. Syst. Dyn., 48 (2010) 457-480.
[16] F. Lu, Q. Gao, J. Lin, F.W. Williams, Non-stationary random ground vibration due to loads moving along a railway track, J. Sound Vibr., 298 (2006) 30-42.
[17] J. Li, J. Chen, The principle of preservation of probability and the generalized density evolution equation, Structural Safety, 30 (2008) 65-77.
[18] J. Li, J. Chen, W. Sun, Y. Peng, Advances of the probability density evolution method for nonlinear stochastic systems, Probabilistic Engineering Mechanics, 28 (2012) 132-142.
[19] Z. Yu, J. Mao, F. Guo, W. Guo, Non-stationary random vibration analysis of a 3d

train–bridge system using the probability density evolution method, J. Sound Vibr., 366 (2016) 173-189.
[20] J. Li, J. Chen, Probability density evolution method for dynamic response analysis of structures with uncertain parameters, Computational Mechanics, 34 (2004) 400-409.
[21] S. Lei, Y. Ge, Q. Li, Effect and its mechanism of spatial coherence of track irregularity on dynamic responses of railway vehicles, Mechanical Systems and Signal Processing, 145 (2020) 106957.
[22] R. Pintelon, E. Louarroudi, J. Lataire, Nonparametric time-variant frequency response function estimates using arbitrary excitations, Automatica, 51 (2015) 308-317.
[23] C.H. Page, Instantaneous power spectra, Journal of Applied Physics, 23 (1952) 103-106.
[24] R.R. Coifman, Y. Meyer, V. Wickerhauser, Wavelet analysis and signal processing, In Wavelets and their applications, Citeseer, 1992.
[25] N.E. Huang, Z. Shen, S.R. Long, M.C. Wu, H.H. Shih, Q. Zheng, N.-C. Yen, C.C. Tung, H.H. Liu, The empirical mode decomposition and the hilbert spectrum for nonlinear and non-stationary time series analysis, Proceedings of the Royal Society of London. Series A: mathematical, physical and engineering sciences, 454 (1998) 903-995.
[26] M.B. Priestley, Evolutionary spectra and non-stationary processes, Journal of the Royal Statistical Society: Series B (Methodological), 27 (1965) 204-229.
[27] M.B. Priestley, Power spectral analysis of non-stationary random processes, J. Sound Vibr., 6 (1967) 86-97.
[28] Y.L. Guo, A. Kareem, Non-stationary frequency domain system identification using time-frequency representations, Mechanical Systems and Signal Processing, 72-73 (2016) 712-726.
[29] A.H. Nayfeh, D.T. Mook, D.W. Lobitz, Numerical-perturbation method for the nonlinear analysis of structural vibrations, AIAA Journal, 12 (1974) 1222-1228.
[30] M. Majji, J.L. Junkins, J.D. Turner, A perturbation method for estimation of dynamic systems, Nonlinear Dynamics, 60 (2010) 303-325.
[31] X. Xiao, Y. Zhang, W. Shen, F. Kong, A stochastic analysis method of transient responses using harmonic wavelets, part 1: Time-invariant structural systems, Mechanical Systems and Signal Processing, 160 (2021) 107870.
[32] X. Xiao, Y. Zhang, W. Shen, A stochastic analysis method of transient responses using harmonic wavelets, part 2: Time-dependent vehicle-bridge systems, Mechanical Systems and Signal Processing, 162 (2022) 107871.
[33] F. Kong, J. Li, Wavelet-expansion-based stochastic response of chain-like mdof structures, J. Sound Vibr., 359 (2015) 136-153.

[34] W. Zhai, X. Sun, A detailed model for investigating vertical interaction between railway vehicle and track, Veh. Syst. Dyn., 23 (1994) 603-615.
[35] S.M. Lei, Y.J. Ge, Q. Li, D.J. Thompson, Wave interference in railway track due to multiple wheels, J. Sound Vibr., (2021) 116620.
[36] T. Wu, D. Thompson, Theoretical investigation of wheel/rail non-linear interaction due to roughness excitation, Veh. Syst. Dyn., 34 (2000) 261-282.
[37] V. Garg, Dynamics of railway vehicle systems, Elsevier, 2012.
[38] X. Song, D. Wu, Q. Li, Dynamic impact analysis of double-tower cable-stayed maglev bridges using a simple model, Journal of Bridge Engineering, 19 (2014) 34-43.
[39] Y.S. Wu, Y.B. Yang, Steady-state response and riding comfort of trains moving over a series of simply supported bridges, Eng. Struct., 25 (2003) 251-265.
[40] J.L. Devore, Probability and statistics for engineering and the sciences, Cengage learning, 2011.
[41] H.L. Yu, B. Wang, C.P. Xia, Z.Y. Gao, Y.L. Li, Efficient non-stationary random vibration analysis of vehicle-bridge system based on an improved explicit time-domain method, Eng. Struct., 231 (2021) 111786.